Domain scaling and marginality breaking in the random-field Ising model

1996 J. Phys. A: Math. Gen. 29 7409

(http://iopscience.iop.org/0305-4470/29/23/011)

J. Phys. A: Math. Gen. **29** (1996) 7409–7438. Printed in the UK

Domain scaling and marginality breaking in the random-field Ising model

E D Moore†§, R B Stinchcombe†‖ and S L A de Queiroz‡¶

† Department of Physics, Theoretical Physics, University of Oxford, 1 Keble Road, Oxford, OX1 3NP, United Kingdom

‡ Instituto de Física, UFF, Avenida Litorânea s/n, Campus da Praia Vermelha, 24210-340 Niterói RJ, Brazil

Received 26 March 1996, in final form 16 July 1996

Abstract. A scaling description is obtained for the d-dimensional random field Ising model, directly from the analysis of domains in a bar geometry. Wall roughening removes the marginality of the $d = 2$ case, giving the $T = 0$ correlation length $\xi \sim \exp(Ah^{-\gamma})$ in $d = 2$, and for $d = 2 + \epsilon$ power law behaviour with $\nu = 2/\epsilon\gamma$, $h^* \sim \epsilon^{1/\gamma}$. Here, γ is one of four rough wall exponents arising in the theoretical formulation. In space dimensionality $d = 2$ the analysis is substantiated by three different numerical techniques (transfer matrix, Monte Carlo, ground-state algorithm). These provide for strips up to width $L = 11$ basic ingredients of the theory, namely free energy, domain size, and roughening data and exponents.

1. Introduction

The phase diagram and critical properties of d-dimensional Ising ferromagnets in a random field has long been a subject of great interest [1–14]. This is partly because the model can be experimentally realized in space dimensionalities $d = 2$ and 3, owing to its correspondence [15] with diluted antiferromagnets in a uniform field [16–28]. Apart from the experimental connection, the random field problem in its own right has challenged theoreticians with rather intricate questions, such as those concerning its lower critical dimension [1, 7–10], the applicability of dimensional reduction [3, 4, 14] and the nature of the transition and critical behaviour [11, 13, 14]. As is well known, the lower critical dimension d_l turns out to be [9, 10] that originally suggested by domain wall arguments [1, 7, 8], $d_l = 2$. This implies a marginal behaviour at dimension $d = 2$, and it has been argued [29–32] that here domain roughening effects are important. This present paper provides a detailed study based on this point of view, extending and complementing basic results presented elsewhere [33]. We explore the consequences of a roughened domain wall picture, and at the same time confirm its validity by observing characteristics of the basic ingredients as well as consequent predicted behaviour in data from numerical studies. While some of the analytical predictions below coincide with those from early work [30–34], our scaling scheme allows for their rederivation in a clear way, with the basic physics always in the foreground.

§ Electronic address: dmoore@thphys.ox.ac.uk
‖ Electronic address: stinch@thphys.ox.ac.uk
¶ Electronic address: sldq@if.uff.br

0305-4470/96/237409+30$19.50

The domain analysis is most conveniently made in a bar geometry. The dependence on a bar width L may be used to arrive at phenomenological scaling transformations. These in turn give the phase diagram and critical properties. For low random field strength h and temperature T, the domains span the bar width, and are well separated along the bar, so the basic 'flat wall' description (without roughening) is very simple. It results, for $d = 2$, in a zero temperature fixed point at which the field scaling is marginal. Adding domain wall roughening breaks this marginality, and this ingredient is essential at and near $d = 2$. Consequences are: (i) the bulk correlation length behaviour $\xi \sim \exp(A/h^{\gamma})$ at $T = 0$ in $d = 2$, and (ii) for $d = 2 + \epsilon$ the phase boundary joining the $T \neq 0$, $h = 0$ fixed point to one at $T = 0$, $h = h^* \sim \epsilon^{(1/\gamma)}$ where $\xi \sim |h - h^*|^{-2/\epsilon\gamma}$. γ is one of four exponents occurring in the h and L dependence of the wall roughening free energy and characteristic scale, and is predicted to be $\gamma = 2$ in the two-dimensional lattice.

This description has been here tested by direct numerical investigations in the bar geometry for $d = 2$ (strips). This is carried out by transfer matrix techniques and by Monte Carlo analysis using a new thermalization technique [35]. In addition, we use data from a max-flow algorithm for constructing ground states [36] which has been adapted for strips.

The domain description involves free energy $\mathcal{F}$ and domain size Ξ as well as roughening characteristics. The largest eigenvalue of the transfer matrix gives accurate numerical data for $\mathcal{F}$, and both $\mathcal{F}$ and Ξ are available from the Monte Carlo analysis, for comparison with the theory. The wall roughening affects both $\mathcal{F}$ and Ξ, but its characteristics are most directly seen in measures of the wall profile itself. These and their associated exponents are best provided by the ground-state algorithm. The resulting comparisons of theory and numerical data give a very complete test of the theoretical description and convincing support for its validity.

The outline of the paper is as follows. In section 2.1 the domain picture is introduced and the flat wall theory is provided at $T = 0$ for the free energy, domain size, and correlation length of bars, and via phenomenological scaling, for the bulk criticality. Section 2.2 generalizes the flat wall description to low temperatures, and section 2.3 describes the numerical approaches and the comparison of free energy and domain size data with flat wall theory. Section 3.1 describes the domain wall roughening at $T = 0$, for lattice and continuum models via a simple approach and a field theory. First, a single 'decoration' is discussed, then decorations on all scales, to provide the modified free energy and domain size, and hence the scaling and criticality. This description is generalized to low temperatures in section 3.2 and compared with the numerical domain size and roughening data, including exponents, from the ground-state algorithm in section 3.3. Section 4 states the main conclusions of the paper.

2. Flat wall

2.1. Zero temperature theory

2.1.1. Introduction. In this section, we establish the domain wall description of the random field Ising model (RFIM) by taking $T = 0$ and assuming flat walls. The results of this simple case are very good in certain ranges of dimensionality, but they indicate also where a more comprehensive picture involving roughening (to be provided in section 3) is required.

We obtain the dispositions of walls by minimizing an energy which is discussed below. The resulting domain size is then used in a phenomenological (finite-size) scaling scheme to provide the renormalization group (RG) transformation and hence the critical properties. Both these steps are most easily carried out in the bar geometry discussed below.

2.1.2. The domain picture. Following Imry and Ma [1] we suppose that the field contribution to the energy of a domain goes like $h\sqrt{V}$ where V is the number of spins within the domain and h is the standard deviation of the field distribution P, assumed to have zero mean. The energy change per domain due to the broken bonds is proportional to the perimeter of the domain A; so

$$\mathcal{F}(T=0) = n_{\mathrm{d}}(2JA - c_0 h\sqrt{V}) \tag{1}$$

where n_{d} is the number of domains. Here A and V represent an average perimeter and volume measurement for all the domains. The basic ferromagnetic energy $-2JNq$ ($q \equiv$ coordination number of the lattice) is neglected throughout this paper. The constant c_0 is of order unity and represents both the statistical fluctuations and the selection effects of the domains. We describe the origins of this constant, and determine its value, in section 2.3.2.

We have chosen the strip geometry in which to apply the zero temperature free energy (1) for the following reasons: (i) convenience for application of finite-size scaling procedures, (ii) amenability to domain wall arguments, and (iii) we wish to later make contact with transfer matrix calculations. Thus we choose a bar geometry ($L^{d-1} \times \infty$), to represent a d-dimensional system. Our analysis gives a length scale $\Xi_L(h)$ which diverges like the correlation length $\xi_L(h)$ at a fixed point h^*. We can then determine the bulk critical properties via an RG equation of the form $h \to h' = R(h)$ which arises from the phenomenological finite-size scaling ansatz

$$\frac{\xi_L(R(h))}{L} = \frac{\xi_{\mathrm{b}L}(h)}{bL}. \tag{2}$$

Standard RG procedures provide, from $R_{\mathrm{b}}(h)$, the critical condition and exponents.

By assuming that at $T = 0$ the only scaling variable is h/J (and for $T \neq 0$ the only additional coupling to be rescaled is T/J, see below), we are taking the traditional view that it is only the variance of the random field distribution that matters. Other quantities, e.g. higher moments of the distribution, might possibly be considered, such as has been done in studies of dilute systems [37]. In not doing so, the system's evolution in parameter space is undoubtedly restricted. However, we expect the restricted evolution to provide the dominant generic behaviour in the present case.

2.1.3. The zeroth-order theory. Given the strip geometry described above, the leading order modification of the ferromagnetic ground state is a splitting of the system into n_{d} domains. These domains are taken to have flat walls that span the width L of the strip and are of typical length Ξ_L, as shown in figure 1. For this picture to be consistent we need $\Xi_L \gg L$, which holds if h is sufficiently small. The lattice constant is set to unity. We may write the excess energy of this domain state (at $T = 0$, equal to the Helmholtz free energy) as

$$\mathcal{F}(T=0) = n_{\mathrm{d}}(2JL^{d-1} - c_0 h\sqrt{\Xi_L L^{d-1}}) \tag{3}$$

where $n_{\mathrm{d}} = N/\Xi_L$. The equilibrium free energy is found by extremalizing with respect to Ξ_L:

$$\Xi_L = L^{d-1}\left(\frac{c_0 h}{4J}\right)^{-2}. \tag{4}$$

Applying the phenomenological scaling equation (2) gives an RG equation for h:

$$h' = hb^{(2-d)/2}. \tag{5}$$

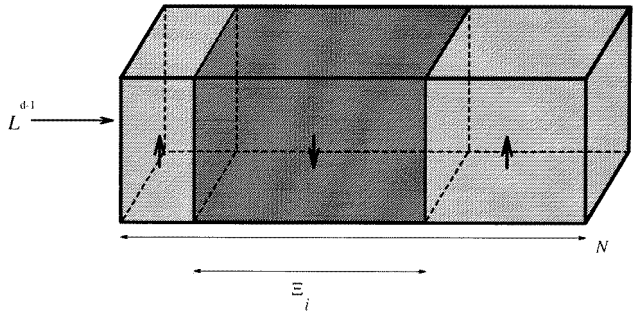

Figure 1. The bar geometry, showing the flat domain walls that separate regions of up and down spins. The average domain size Ξ_L is the average of the Ξ_is.

This implies that there is a fixed point at $h = 0$ which is unstable for $d < 2$ and stable for $d > 2$. See [34] and references therein for early derivations of this. Thus, for $d < 2$ the critical exponent $\nu = 2/(2-d)$ for the unstable fixed point at $h = 0$. At $d = 2$ the scaling field h is marginal. Higher-order terms in the free energy, however, can break this marginality. The wall roughening decorations described in section 3 achieve this.

2.1.4. The correlation length at $T = 0$. In a bar geometry, the correlation length ξ_L controls the exponential decay of the configurationally averaged correlation function. It is easy to show (assuming independently randomly distributed flat domain walls), that ξ_L is related to the domain size Ξ_L by

$$\xi_L = \left[\ln\left(\frac{1}{1-2/\Xi_L}\right)\right]^{-1}. \tag{6}$$

For large Ξ_L this gives $\xi_L = \Xi_L/2$, a proportionality to be intuitively expected.

Assuming a flat wall picture, ξ_L, of the RFIM on a strip can actually be found exactly at $T = 0$ (for a binary distribution of random fields). This generalizes the work of Farhi and Gutmann [38] for the one-dimensional RFIM.

The key is to consider the connected correlation function

$$\chi_{il} = \langle\sigma_i\sigma_{i+l}\rangle - \langle\sigma_i\rangle\langle\sigma_{i+l}\rangle \tag{7}$$

where angled brackets denote the usual thermodynamic average and σ_i and σ_{i+l} are any two spins in columns i and $i+l$, respectively. Owing to the discrete, binary field distribution one may view the random field configuration on a strip of width L as a random walk in $1+1$ dimensions [38].

At $T = 0$ the thermodynamic average becomes an average over the possible ground states of the system. The fact that the ground state is degenerate is due to the discrete ($\pm h$) field distribution used here; for a continuous distribution it can be shown [39, 40] that the ground state is unique, thus $\chi_{il} \equiv 0$.

The details of the calculation thus suggested are presented in appendix A, with the end result that, for small field h, one has:

$$\begin{aligned}\xi_L &= \frac{1}{L\ln\cos(\pi/(2J/h+2))} \\ &= 2L\left(\frac{2J}{\pi h}\right)^2 + \frac{16\pi^2}{h} + \mathcal{O}(1).\end{aligned} \tag{8}$$

It is easy to generalize these arguments to higher dimensions via the replacement $L \to L^{d-1}$. Then (8) agrees to highest order in h with our earlier result for the $T = 0$ small h correlation length (from combining (4) with (6)). However, this result came from an analysis of the *connected* correlation function, whereas our prior analysis applied to the *disconnected* correlation function. Although the correlation lengths derived from these two quantities should diverge in the same manner, they may differ by a multiplicative constant (e.g. c_0). Indeed, this turns out to be the case in section 2.3.

Although this calculation also assumes a flat wall scenario, it should be accurate when $\xi_L \gg L$ and is exact for $L = 1$.

2.2. Low-temperature theory

The extension of the domain wall analysis to non-zero temperature requires the construction of an entropy to be used in the minimization of the free energy $\mathcal{F} = U - TS$, in order to determine the characteristic lengths for phenomenological scaling. In the low-field, low-temperature limit we can use the well separated strip-spanning domain pictures developed in the previous section. For the zeroth-order (flat wall) description, the entropy is quite trivial, corresponding to the number of ways of laying down flat domain walls with an average spacing $\Xi_L = N/n_\mathrm{d}$:

$$S_0(\Xi_L) = \ln \binom{N}{n_\mathrm{d}} = N \left[\frac{\ln(\Xi_L - 1)}{\Xi_L} - \ln(1 - \Xi_L^{-1}) \right] \tag{9}$$

with $k_\mathrm{B} = 1$ and using Stirling's approximation. The free energy generalizing (1) to $T \neq 0$ is then

$$\mathcal{F} = n_\mathrm{d}(2JL^{d-1} - c_0 h \sqrt{\Xi_L L^{d-1}}) - TS_0(\Xi_L). \tag{10}$$

Extremalizing with respect to Ξ_L gives the following equation for the domain size

$$-2JL^{d-1} + \frac{c_0 h}{2} L^{(d-1)/2} \Xi_L^{1/2} + T \ln(\Xi_L - 1) = 0. \tag{11}$$

The various limits of this equation are

$$\begin{aligned} \Xi_L &= \left(\frac{4J}{c_0 h} \right)^2 L^{d-1} \qquad T = 0 \\ \Xi_L &= 1 + \exp\left(\frac{2JL^{d-1}}{T} \right) \qquad h = 0. \end{aligned} \tag{12}$$

As a check on equation (12), we investigate the low-temperature behaviour of the zero-field Ising model. By using this form for Ξ_L in equation (2) we get the recursion relation for T/J

$$(T/J)' = \frac{2L^{d-1}(T/J)}{2(bL)^{d-1} - (\ln b)(T/J)}. \tag{13}$$

This has a fixed point at $T = 0$ which is unstable for $d \leqslant 1$ and stable for $d > 1$, in the latter case consistent with a finite T_c. In $d = 1$, (12) gives the usual pure Ising result $\xi \sim \exp(2J/T)$.

Thus, in $d = 1$ the two scaling variables (scaling like a length) are $\exp(2J/T)$ and (from (5)) $h^{-2/(2-d)}$. In $d = 1$ the correlation length can then be written in the crossover form

$$\xi = \mathrm{e}^{2J/T} \phi(h^2 \, \mathrm{e}^{2J/T}) \tag{14}$$

where $\phi(x) \to c_a$ or c_b/x for $x \to 0$ or ∞, respectively, with c_a, c_b constants.

For $d > 1$ the stability with respect to temperature of the $(T, h) = (0, 0)$ fixed point means that no crossover form then applies at low T, h, but instead $h^{2/(2-d)}T^{1/(d-1)}$ is invariant under scaling. Such stability also implies that the thermal scaling has little influence on the low T, low h critical behaviour for $d > 1$. Nevertheless, thermal effects contained in (10) and (11) can substantially modify the behavour of the free energy and domain size in this regime, masking the field dependences more significant for the RG scaling. So (10) and (11) will be required for interpretations in the next section, where numerical techniques are used to confirm the basic scaling picture so far discussed.

2.3. Numerical evaluation

2.3.1. Introduction. The most obvious test of the theory is on its final scaling predictions for the bulk system criticality. However, this is difficult since it requires the investigation of a system large enough to show the bulk critical behaviour. It is much easier to apply the numerical techniques to the finite-size strip geometry, as is done here, and to investigate the non-critical ingredients from which the scaling transformation is built, and hence establish the applicability of the basic flat wall procedure.

Three techniques have been found to be successful, with results reported below: a transfer matrix calculation, a modified Monte Carlo simulation, and a ground-state algorithm.

The transfer matrix method is appropriate to the strip geometry and can, in principle, provide the phenomenological RG transformations directly and very precisely, as has been exemplified for many low-dimensional lattice systems, particularly those with non-random transfer matrices.

Very accurate results have also been obtained for the random bond Ising model and a modification of those techniques is used here [41]. Because of the quenched disorder present in such models (and in the RFIM), the first (dominant) Lyapunov exponent of the transfer matrix product gives the average free energy of the strip, which is one of the two key ingredients in our domain wall analysis. The other ingredient is the domain wall size or correlation length. Typically, the correlation length is provided by the TM approach via

$$\xi_L = \frac{-1}{\ln(\lambda_1/\lambda_0)} \tag{15}$$

where λ_0 and λ_1 are the largest and second largest eigenvalues, respectively. However, this relation gives the *most probable* correlation decay [42], which need not be the same as the *average* correlation decay. In fact, the correlations may follow quite complex distribution functions [42], and the difference between 'most probable' and 'average' decays becomes especially important when the effective interactions may differ in sign, such as in spin glasses or random field problems [42, 43]. For this reason, the comparison with transfer matrix data will be restricted to the free energy.

Monte Carlo simulation is the second technique used. The usual equilibriation problems set by critical slowing down are here compounded by the effects of very large energy barriers in situations ($d \leqslant 2$) where the criticality is at $T = 0$. The problems are partly alleviated by the strip geometry, particularly in $d = 2$, where characteristic lengths of order h^{-2} (see (4)) replace exponentially large correlation lengths of the bulk system (see (48) below). However, the equilibriation times remain excessively long, and a new algorithm [35] was devised and employed to markedly improve thermalization times. Briefly, this algorithm continues the ideas of multigrid methods with self-adjusting renormalizations of parameters to allow for changes to be made on all length scales via moves of blocked spins. This permits

the calculation of average energies, domain sizes, and correlation lengths, for comparison with the analytic predictions.

The final numerical technique used was an exact algorithm [44] to construct the ground states for both binary and Gaussian random-field configurations. Ground states for models with arbitrary random fields and arbitrary but not frustrated exchange interactions may be found in polynomial time by mapping the optimization problem to a min-weighted-cut problem on an associated graph [45]. A new min-cut max-flow algorithm [44] was first implemented by Ogielski [36] to demonstrate the practicability of this method. We here apply the algorithm to the strip geometry, and hereafter refer to this method as the 'max-flow algorithm'. From these data it was possible to obtain $T = 0$ properties including average energy, domain size, as well as domain wall roughening characteristics which will be discussed later.

2.3.2. Transfer matrix. The simulations were done on strips of width $L = 2, \ldots, 9$ and length $N = 10^5$ and a binary random field distribution. Periodic boundary conditions were applied in the 'finite' direction whereas all possible trial state vectors were applied to termini of the strip at each end of the 'infinite' direction. This procedure was then repeated for three different realizations of the random field configuration, and the resulting free energy

$$\mathcal{F}/N + 2 = -kT \ln \lambda_0 \tag{16}$$

averaged over these realizations and over the 2^L trial vectors. The average was calculated in the root-mean-square manner, and the associated error in the free energy was calculated as the rms error in the free energy at each random field configuration.

We wish to test the zeroth-order flat wall theory (section 2.1), in which the free energy at very low temperature and $d = 2$ is

$$\mathcal{F}_0 = -\frac{Nc_0^2h^2}{8LJ}. \tag{17}$$

To this end, we have generated free energy data $\mathcal{F}_{\mathrm{TM}}$ for $L \in (2, 7)$ at $T = 0.1J$. For lower temperatures, the elements of the transfer matrix become larger than the computer can handle. If the strip width is much larger than 7 the run times become unreasonably long. Nevertheless, these strip widths are adequate for our purposes.

We plot $\ln(\mathcal{F}_{\mathrm{TM}}/J)$ versus $\ln(h/J)$ for various strip widths L. Straight lines of slope 2 are expected, and this is indeed the case, as demonstrated in figure 2.

Straight line fits to these plots yield the slopes given in table 1. We include the value of the Q statistic, which is a measure of the probability that a value of χ^2 as *poor* as the value we have found should occur by chance. Q is always in the range $(0, 1)$ and a value of $Q > 0.1$ usually denotes a reliable fit [46].

The agreement is acceptable, with increasing accuracy at larger L. However, close inspection of figure 2 shows that there appear to be systematic errors. This is an indication of the importance of higher-order decoration effects and finite-temperature effects, occurring even at these low temperatures and low fields.

We now attempt to obtain a best value for the constant c_0, so that we can compare the predicted free energy with the numerics, and extract subdominant features noted above. We defer a comparison of estimates of c_0 obtained by different numerical procedures to the end of section 2.3.

A simple fit of the numerical free energy to equation (17) is statistically unreliable, and gives residual L dependence in c_0, and other artifacts. We concluded that this was due to the data being at $T = 0.1J$ and not zero temperature. For small h, the leading temperature

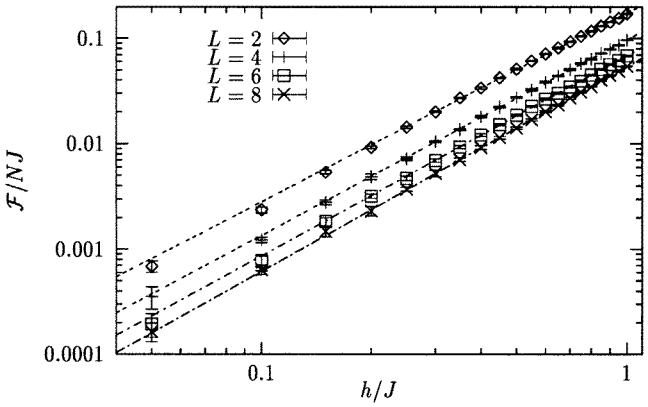

Figure 2. Log–log plots of the excess free energy at $T = 0.1J$.

Table 1. Fits to the free energy data from the transfer matrix.

L	Slope	Error	Q
2	1.792	0.007	0.0004
3	1.848	0.009	0.33
4	1.857	0.009	0.79
5	1.885	0.011	0.96
6	1.901	0.012	0.95
7	1.904	0.012	1.00
8	1.945	0.015	1.00
9	1.958	0.014	1.00

dependence can be very significant. Indeed, the zeroth-order finite temperature theory of (10) and (11) implies that for large Ξ_L in a two-dimensional lattice

$$\mathcal{F} = -N\frac{c_0^2h^2}{8LJ}\left[1 + \mathcal{O}\left(\frac{T}{LJ}\ln\left[L\left(\frac{4J}{c_0h}\right)^2\right]\right)\right]. \tag{18}$$

To fit the free energy data properly, we need a free energy form applying for all h, T as long as Ξ_L is large. This can be obtained by reparametrizing the relations (10) and (11) giving the finite temperature flat wall theory, provided the theory is correct for large Ξ_L. Using h, T small, Ξ_L large, $d = 2$, the approximate forms to reparametrize are the excess free energy

$$\frac{\mathcal{F}}{\mathcal{N}L} \equiv f = \frac{-c_0h}{2\sqrt{\Xi_L L}} \tag{19}$$

and the extremalizing equation

$$\left(\frac{c_0hL^{1/2}}{4T}\right)\Xi_L^{1/2} + \frac{1}{2}\ln\left(\Xi_L\exp\left(\frac{-2JL}{T}\right)\right) = 0. \tag{20}$$

This leads to an implicit equation for f as a function of h, T, L

$$\frac{LJ}{T} = \ln\left(\frac{-c_0h}{2f\sqrt{L}}\right) - \frac{c_0^2h^2}{8fT} \tag{21}$$

which is solved for f numerically, thus determining c_0.

As well as obtaining c_0, we can test whether non-Gaussian effects occur for small L, or perhaps the flat wall description breaks down for large L by varying the range of the fit. We used $T/J = 0.1$, 0.2 and 0.3, with $h \in \{0.05, 0.25\}$. Over this range of T and h, the zeroth-order theory predicts large correlation lengths at least $> 10L$ for even a liberal estimate of c_0, which should make (21) applicable. The results are presented in table 2.

Table 2. Fits of the free energy to the transfer matrix data at finite temperature.

L	c_0	χ^2	Q
2–9	1.774	457	10^{-41}
2–7	1.761	375	10^{-37}
2–5	1.745	288	10^{-32}
4–9	1.846	81	0.686

The fits improve by a large amount when the lower L values are dropped ($Q = 0.686$ is remarkably good). We attribute this to non-Gaussian selection effects at lower L values, where the domains do not sample over as many field configurations as a domain of the same linear extension at large L.

The value $c_0 \approx 1.85$, found here does not agree with that ($c_0 = \pi$) predicted in section 2.1.4 by a random walk analysis of the disconnected correlation function. As explained there, this is due to the different correlation functions used in obtaining this (non-universal) constant.

The large Q statistic gives much confidence in the form of $\mathcal{F}$ predicted from the flat-wall ansatz. Figure 3 illustrates the quality of the agreement between the transfer matrix data and the prediction of equation (21) using $c_0 = 1.85$. While the fits were done for $h \in (0.05, 0.25)$, the predicted free energy seems to lie within error for a much larger regime, especially for larger strip widths. For $L = 8, 9$ this happens all the way out to $h = 1.0J$.

Transfer matrix data were also taken for $h/J \in (1, 6)$ and low T. Typical results are shown in figure 4. For $h/J \in (0, \approx 2)$, $\mathcal{F}$ goes roughly like h^2. This dependence is close to that predicted by the flat-wall theory, with increasing accuracy as the strip width increases, which is important for our scaling discussion of critical effects. For $h/J > 4$ the field strength is greater than the energy cost of flipping a spin, so all the spins align with their local field. Thus $\mathcal{F}$ is linear in h, with unit slope. In the intermediate region $h/J \in (\approx 2, 4)$ $\mathcal{F}$ crosses over from quadratic to linear dependence on h, due to a rapidly decreasing domain size.

The transfer matrix approach has thus provided a rigorous test of the energetic arguments of sections 2.1.3 and 2.2, with excellent agreement over the range tested.

However, a comparison of quantities like correlation length, domain size, etc, would be a more rigorous check on the physics underpinning the results. Secure results on these lengths are not so far available from the transfer matrix method and so we turn to the Monte Carlo analysis.

2.3.3. Monte Carlo. Using the block Monte Carlo algorithm described in [35] we now investigate other physical quantities which are directly accessible via our theoretical framework, but not easily obtained by transfer matrix analysis.

The average energy: First, we compare the configurationally averaged energy found by the Monte Carlo routine to that predicted by the flat wall results (the first term in (10)),

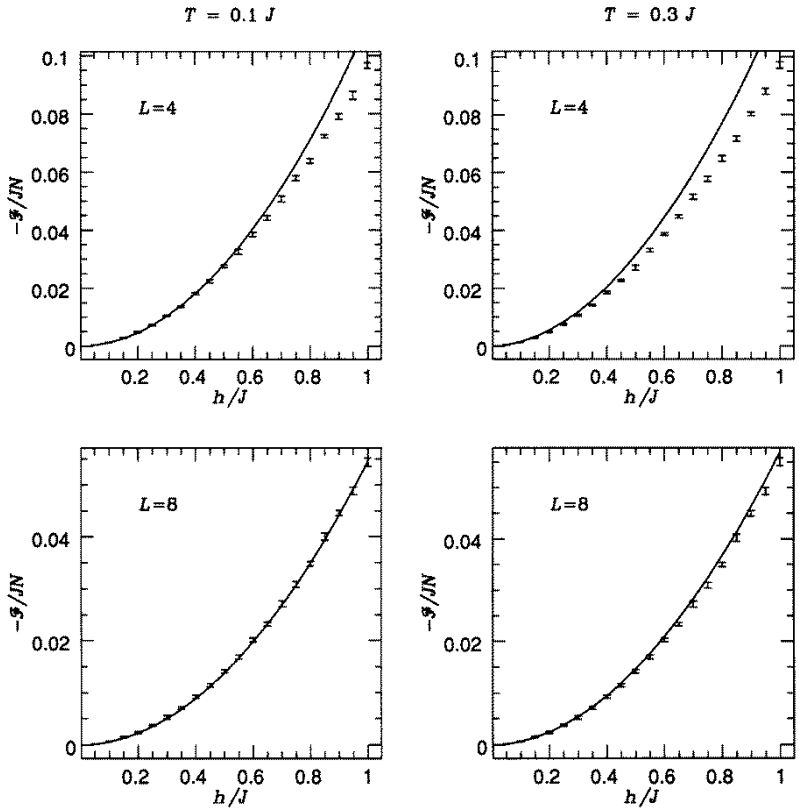

Figure 3. A comparison of the free energy as determined by the transfer matrix data, and that determined by our low-temperature theory using the fitted constant $c_0^2 = 3.406$, at $T = 0.1J$ and $T = 0.3J$.

which involves Ξ_L as given by numerical solution of (11). The theoretical and Monte Carlo data points are shown for $L = 1$ and 4 in figure 5.

Fitting the data to the theoretical form (3) gives $c_0 = 1.75 \pm 0.05$. The theory agrees quite well with the Monte Carlo data for low temperature and field strength, as the criterion for the validity of the theory breaks down when $\Xi_L \approx L$. Yet, there is agreement within error up to $T = 0.7J$ even for $h = 0.5J$ when $L = 4$. This is a further indication that the zeroth-order theory captures the essential flavour of the RFIM.

The domain distribution and correlation length–domain size relationship: A key assumption in our theory was that the domain walls were randomly placed on the strip. This can be tested either by investigating the domain size distribution, which should then be Poisson, or by exploring the predicted relation between domain size and correlation length.

Since the standard deviation and mean of a Poisson distribution are the same, we have evaluated these two quantities for $L = 1, 2$ and 4 for $h \leqslant 0.5J$ and $T \leqslant J$. In every case they are found to be the same within error (never more than 5%). While this result is not definitive, it is very suggestive of a Poisson distribution.

Equation (6) expresses the relation between the correlation length ξ_L, and the domain size Ξ_L, for randomly distributed walls. Figure 6 shows a test of this relationship for $L = 2$.

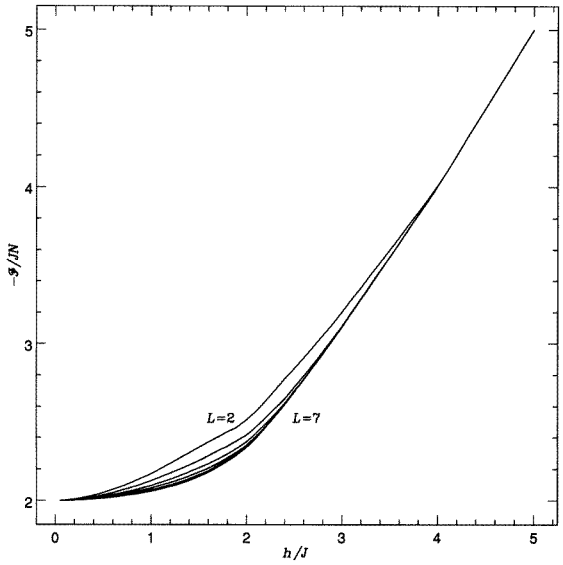

Figure 4. The free energy as a function of h for $T/J = 0.1$ and $L \in (2, 7)$. These data were determined by the transfer matrix method, and illustrate the three regimes of h dependence.

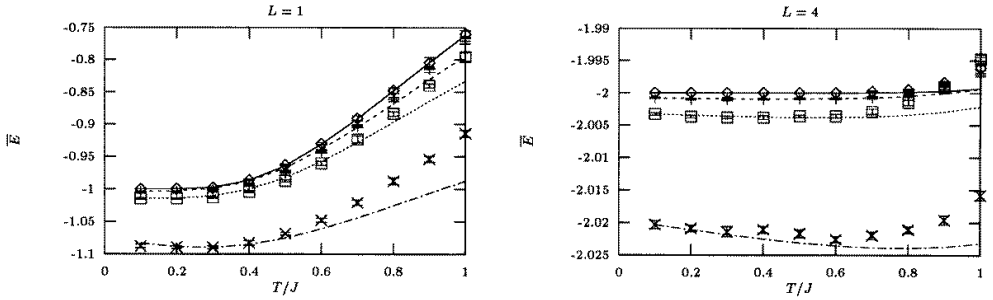

Figure 5. The average energy of the $L = 1$ and $L = 4$ RFIM, as determined by both the Monte Carlo algorithm (data points) and the zeroth-order theory (lines). The symbol $\diamond$ corresponds to $h = 0$, $-$ to $h = 0.1J$, $\square$ to $h = 0.2J$ and $\times$ to $h = 0.5J$.

Very similar plots arise for $L = 1$ and 4. In each case, the agreement with the predicted form is remarkable.

We have also analysed the probability distribution of domain sizes for $L = 1, 2, 4$; $h = 0, 0.2J$ and T up to J. The results for $L = 1$ are shown in figure 7. The size distribution is very close to exponential (consistent with the domains being Poisson distributed) for $h = 0$, at least for smaller L's and larger temperatures. However, when $h = 0.2J$ and $T = 0.4J$ the distribution seems to decrease at lower Ξ. This is evidence for *domain wall repulsion*, which is expected at higher fields when the domain walls begin to approach and undergo appreciable roughening (see section 3). For $h < J$, however, this effect is only noticeable over about the lower 2% of the domain size distribution. Otherwise, the distribution is still exponential. So, the Poisson assumption appears to be approximately correct, and gives the correct behaviour at large domain sizes. Thus, the flat wall entropy should still be a valid starting point.

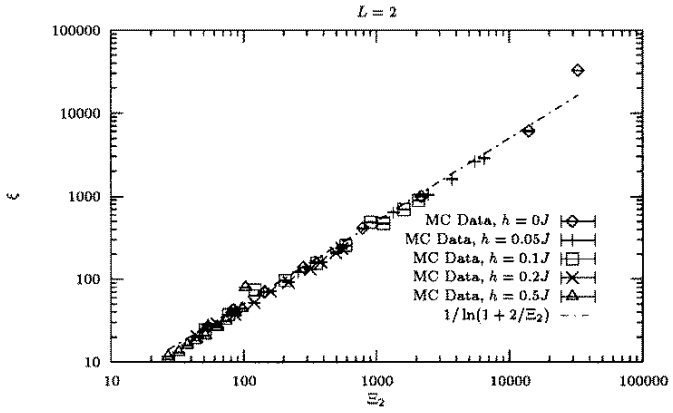

Figure 6. The correlation length ξ_L plotted against the domain size Ξ_L for $L = 2$. We also include the predicted relation between these quantities for comparison. Plots for $L = 1, 4$ are essentially the same.

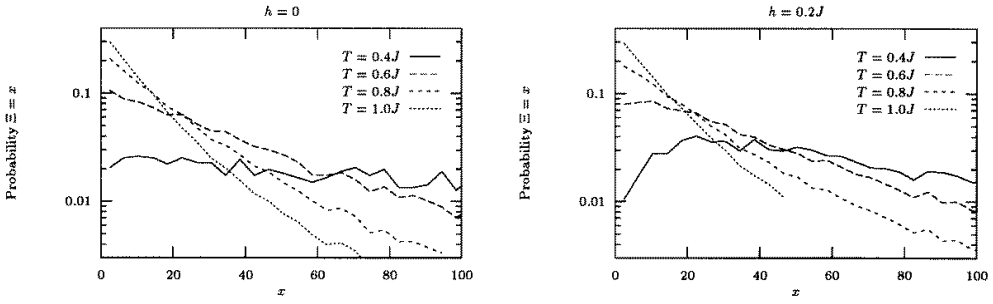

Figure 7. The distribution of domain sizes according to the measure Ξ_L as found by the Monte Carlo routine when $L = 1$.

The domain size itself: In this section, the domain size Ξ_L, predicted by (11) is compared with that measured by the Monte Carlo routine.

The results are shown for $L = 1$ and 4 in figure 8. The flattening of the data at low T's is due to the finite length of the simulated system; data in the flattening regime are discarded in quantitative comparisons. The constant c_0 was determined by a best fit to the data at $T = 0.1J$, where we might expect the flat-wall theory to be accurate. We get $c_0 = 1$.

The comparison of the predictions of (11) to the domain size data is relatively poor. The reason for this is not well understood, but may be due to non-Gaussian effects at smaller strip widths. However, we do get reasonable agreement (discarding flattened data) at the lowest of temperatures, and for larger L. These are the conditions that matter most for scaling, where the correlation length and domain size at $T = 0$ and large L is of particular importance. These are discussed below using data from the ground-state algorithm.

2.3.4. Max-flow algorithm. We have used the max-flow algorithm [36] to find ground states and ground-state properties for random field configurations generated from binary or Gaussian distributions. On large scales, both distributions are expected to give the same results, but there are differences, discussed in section 3.3, for small system or domain sizes. These differences were not as pronounced in the finite T data obtained from the

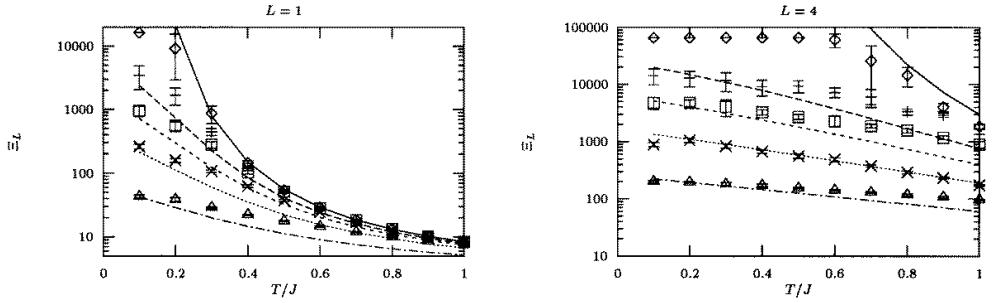

Figure 8. The domain size Ξ_L plotted as a function of temperature for $L = 1$ and $L = 4$. The data points represent the Monte Carlo data whereas the lines show the result of solving the flat wall theory. The symbol $\diamond$ corresponds to $h = 0$, $-$ to $h = 0.05J$, $\square$ to $h = 0.1J$, $\times$ to $h = 0.2J$, and $\triangle$ to $h = 0.5J$. The flattening of the data at low T is due to the finite length of the simulated system.

transfer matrix and Monte Carlo routines described above. In the present case, it becomes advantageous to use results from the Gaussian distributions as we now do.

These data were generated on strips of width $L = 2, \ldots, 11$ and length $N = 10^3$, averaged over 100 independent random field configurations. The error bars shown represent the statistical variations in the data when averaged over these runs (as opposed to the width of the distribution of a variable quantity like the domain size). As the computational time required to generate a ground state via this algorithm grows like n^3, and the run time for an $n = 11 \times 10^3$ system was on order 10 days, it was not possible to significantly increase the system size beyond this limit.

The typical domain size Ξ_L is shown in figure 9. Also shown is a comparison with the theoretical Ξ_L obtained from the random walk analysis (section 2.1.4) of the correlation length ξ_L using a simple fitted constant of proportionality to convert this to a domain size. A quantitative assessment of the quality of the agreement is provided by the correlation coefficient $r = 0.9968$ and the statistic $\chi^2 = 0.426$. The fit gives a value of $c_0 = 1.98 \pm 0.02$.

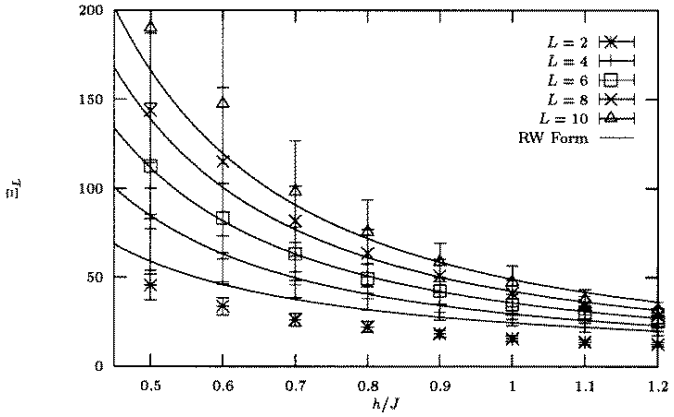

Figure 9. The typical domain size at $T = 0$ from the max-flow algorithm. The points represent the data from the max-flow algorithm, and the full curves represent the theoretical form with a fitted multiplicative constant.

Also considered was a fit to just the h^{-2} leading term in the small h expansion of the theoretical Ξ_L. This corresponds to (4) (i.e. to the basic $T = 0$ theory) and differs from the full Ξ_L by $\mathcal{O}(1/h)$, significant except in the low h limit. The comparison of fits to this reduced form with those to the full Ξ_L shows that if fields up to $h = 2.0J$ are included, the fit to the reduced form gives a $\chi^2 = 4.215$. This shows a much poorer quality of fit than that to the full theoretical form. The neglect of the $\mathcal{O}(1/h)$ terms is one of the sources of the reduced quality fit observed in the basic theory analysis of the Monte Carlo domain size data (section 2.3.3). However, it is difficult to incorporate these higher-order terms in a consistent finite-temperature theory. This shortcoming disappears in the small h regime important for scaling.

We get four differing numerical estimates of c_0, namely: 1.85 from transfer matrix data for the free energy; 1.75 ± 0.05 from Monte Carlo average energy; 1 from Monte Carlo domain sizes; 1.98 ± 0.02 from the ground-state max-flow algorithm. Each error bar quoted reflects uncertainties in the fit of c_0 as measured by a specific method; it does not account for systematic errors that may be present, owing to approximations inherent to that particular method. The scatter among estimates is most likely due to this latter source, though at present we are unable to elaborate on this point.

This completes the comparisons of numerical analyses with the basic theory. The conclusion is that this theory provides an excellent account of the free energy and average energy; and an account of the domain size and correlation length which differs from the numerical data by effects whose origin is becoming clear, particularly so at low temperature. These effects are the domain wall repulsion due to non flat wall effects (wall roughening), seen in the domain distribution of section 2.3.3, and the (understood) $\mathcal{O}(1/h)$ and other terms by which the basic theory differs from the random walk one. Thus it is necessary to extend the theory by including wall roughening effects, which is done in the next section.

3. Domain wall roughening

3.1. Theory

3.1.1. Introduction. The effect of domain wall roughening on the free energy, and hence the correlation length is estimated here by a decoration method. Initially, for completeness we rederive expressions which are valid for individual decorations on a given scale a (presumably in a bulk system) [8, 47, 48]; our ultimate goal is to relate the superposition of these to the finite width of our systems, via the upper cutoff L, and thus investigate their effect on the RG transformations: as it turns out, new terms arise which break the marginality of $d = 2$. Hence, we can derive the scaling behaviour in $d = 2$, and the critical point and critical exponents of the RFIM in $d = 2+\epsilon$. All these calculations are carried out at zero temperature for simplicity, and will be later generalized to finite temperature. It is to be noted from the outset that the picture of decorations upon decorations to be developed in section 3.1.3 implicitly allows for the existence of interface overhangs (though not 'bubbles') when one considers the lattice case, or even in the continuum provided that there is sufficient curvature (see figure 10).

For a single decoration base length a and height $b(a)$ the associated excess volume δV and the excess area δA are, on a d-dimensional lattice

$$\delta V = ba^{d-1} \qquad \delta A = 2(d-1)ba^{d-2}. \tag{22}$$

In a continuum, assuming axial symmetry, we denote the excursion of the domain wall from its mean position as $z = bf(r/a)$ where $f(0) = 1$. Then, the excess surface area in

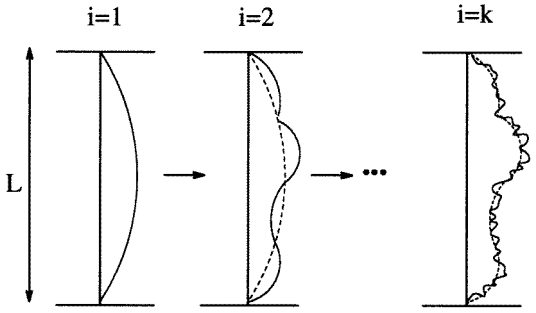

Figure 10. The process of placing decoration upon decorations, such that decorations occur on all length scales. This process has a cutoff length scale when the size of the decorations becomes an order of the lattice constant.

the free energy (1) is

$$\delta S(a,b) = \int_0^2 \mathrm{d}r\, r^{d-2}\left(\sqrt{1+\left(b\frac{\partial}{\partial r}f\left(\frac{r}{a}\right)\right)^2}-1\right)$$
$$\rightarrow \begin{cases} b^2 a^{d-3} & \text{if } b \ll a \\ b a^{d-2} & \text{if } b \gg a. \end{cases}$$

Similarly, the excess volume is

$$\delta V(a,b) = \int_0^a \mathrm{d}r\, r^{d-2} b f\left(\frac{r}{a}\right) \sim b a^{d-1}. \tag{23}$$

We assume that the domains are sufficiently large and the domain wall fluctuations sufficiently small (i.e. $\Xi_L \gg b$) that the fluctuations in the wall may be considered as uncorrelated from those in the body of the domain. Thus, we may treat the decoration as a separate entity from the bulk of the domain and apply the free energy (1) independently to it.

We define the wandering exponent ζ, the free energy fluctuation exponent θ, and associated exponents γ and κ by the following equations

$$\delta\mathcal{F} \sim h^\gamma a^\theta \tag{24a}$$
$$b \sim h^\kappa a^\zeta. \tag{24b}$$

Below, we proceed to the calculation of these four exponents for both lattice and continuum systems.

Substituting (22) into equation (1) the zero temperature excess free energy is, for the lattice

$$\delta\mathcal{F}(T=0) = 4J(d-1)ba^{d-2} - c_0 h b^{1/2} a^{(d-1)/2}. \tag{25}$$

Minimizing with respect to b we get

$$b = \left(\frac{c_0 h}{8J(d-1)}\right)^2 a^{3-d}. \tag{26}$$

The excess free energy is then

$$\delta\mathcal{F}(a) = \frac{-c_0^2 h^2}{J}\frac{a^{3-d}}{16(d-1)}. \tag{27}$$

For the continuum, minimizing (1) with respect to b yields the following relations

$$b \sim \left(\frac{h}{J}\right)^{2/3} a^{(5-d)/3} \qquad \text{if } b \ll a \tag{28}$$

$$b \sim \left(\frac{h}{J}\right)^{2} a^{3-d} \qquad \text{if } b \gg a. \tag{29}$$

For self-consistency, in the continuum case we must require that (28) holds at large scales a only for $d > 2$ and that h/J is not much larger than unity, or that $d = 2$ and $h/J \ll 1$. Similarly, equation (29) only holds if $d < 2$. We now check the assumption that the wall decorations are decoupled from the bulk of the domains, i.e. that $b(L) \ll \Xi_L$. Using the form of Ξ_L given by the zeroth-order decorations (4) and the solutions for $b(L)$ given in equations (28) and (29) above we conclude that h/J must satisfy

$$\frac{h}{J} \ll \begin{cases} L^{(d-2)/2} & \text{if } b \ll a \\ L^{(d-2)/2} & \text{if } b \gg a. \end{cases} \tag{30}$$

In either case then, for large L and $d \geqslant 2$ there is a generous regime for h/J which satisfies the assumption. When $d < 2$, if L is finite we can always find h/J sufficiently small that (30) is satisfied, but the allowed regime for h/J decreases as L increases.

For the continuum the free energy is thus given by

$$\delta\mathcal{F}(a) \sim \begin{cases} -\dfrac{h^{4/3}}{J^{1/3}} a^{(d+1)/3} & \text{if } d \geqslant 2 \\ -\dfrac{h^2}{J} a & \text{if } d \leqslant 2 \text{ and } h \ll 1. \end{cases} \tag{31}$$

The above results have been derived previously [7, 29, 30, 47, 48]. Though the fact that lattice and continuum exponents differ seems surprising at first, it has been shown by Nattermann [47, 48] that for $d \leqslant 3$, if one considers the appropriate relationships between microscopic and mesoscopic parameters the results from both approaches coincide when considered on sufficiently large scales.

3.1.2. Full field theory and comparisons. A more complete treatment of this problem allows the entire shape of the interface to be determined by the system, and not just the height to width ratio as in the previous treatment. This will provide a check on the results of the previous section, as well as more detailed information on the average equilibrium shape of the domain walls, and on proportionality constants.

A functional equation can be established for the shape of the interface by rewriting the free energy of the domain wall as a functional of the wall profile P. The equilibrium wall profile is then found by extremalizing this free energy via the Euler–Lagrange equation. Details of the calculation are found in appendix B. The results of this section, which hold only in $d \geqslant 2$, are:

(1) the first-order free energy fluctuation is given by

$$\mathcal{F}_{\text{wall}}(L) = -\tilde{c}\left(\frac{c_0 h}{J}\right)^{4/3} L^{(d+1)/3} + \mathcal{O}(h^{8/3}) \tag{32}$$

where $\tilde{c}$ is a positive numerical constant, thus showing that wall roughening is always favourable for $d \geqslant 2$;

(2) the wall wandering height is

$$b \sim h^{3/2} L^{(5-d)/3} + \mathcal{O}(h^{8/3}). \tag{33}$$

We now compare the results from lattice theory, simple continuum ansatz and full field theory. One sees that all the exponents of the simple continuum ansatz and the full field theory agree for $d \geqslant 2$. The complete comparison between all three treatments is given in table 3.

Table 3. Comparison of approaches to wall decoration problem.

	$d < 2$			$d \geqslant 2$		
	Lattice	Simple continuum	Field theory	Lattice	Simple continuum	Field theory
ζ	$3-d$	$3-d$	NA	$3-d$	$(5-d)/3$	$(5-d)/3$
θ	$3-d$	1	NA	$3-d$	$(d+1)/3$	$(d+1)/3$
γ	2	2	NA	2	4/3	4/3
κ	2	2	NA	2	2/3	2/3

As mentioned above, the predicted exponents have been found previously; in the continuum model, via other extensions of the Imry–Ma type argument done by Natterman [12, 47, 48], and for the lattice in the work of Binder [30]. Grinstein [49], finds the same values for γ, κ, and ζ as we do, but finds $\theta = 1$. It is also worth noting that the replica symmetric approach of Parisi and Sourlas [50] for the continuous model gave $\zeta = (5-d)/2$, but the inclusion of replica symmetry breaking gives $\zeta = (5-d)/3$ [51, 52]. Finally, the lattice result is consistent with the results of transfer matrix calculations done in two dimensions by Fernandez *et al* [53] and with numerical ground-state calculations reported in section 3.3.

3.1.3. Decorations upon decorations. The decoration described in section 3.1.2 is (to lowest order in h/J), the most favourable twice differentiable form of the domain walls. However, discontinuities may be a feature of the 'true' solution. We may incorporate such discontinuities by allowing the decoration to be repeated on all length scales, following a procedure of Binder [30]. Basically, having made a basic change in the shape of the domain wall on scales of length L, one then looks at the domain wall on a length scale L/n where $n > 1$ is some arbitrary integer, whose choice, we hope, should not strongly affect the results. Here L is the transverse width of the bar. If the random field is small, the wall will be slowly varying on such a scale and may be viewed as a hyperplane, or to preserve the simplicity of the discussion by taking $d = 2$, as a straight line. This straight line is then decorated in the same manner as the original wall. This process is repeated on length scales of order $a_i = L/n^i$, $i = 2, 3, \ldots$ until a cutoff length scale is reached (see figure 10). Reverting to general d, this cutoff occurs at a stage k where the smallest length scale of decorations is the lattice constant (unity), i.e.

$$\min(a_k, b_k) = 1. \tag{34}$$

From the results of the previous section, we know that $b_k = c_1(h/J)^\kappa a_k^\zeta$ where c_1 is a constant. As $\kappa > 0$, (34) becomes $b_k = 1$ for small h so the final level of decorations, k, is determined by

$$a_k = L/n^k = c_1^{-1/\zeta} h^{-\kappa/\zeta}. \tag{35}$$

This gives the cutoff k as

$$k = \frac{\ln L + \frac{1}{\zeta}\ln c_1 h^\kappa}{\ln n}. \tag{36}$$

This result should be approximately valid for large L.

Finally, all the changes to the free energy from all the various decorations are summed to arrive at a total decoration. At stage i we have decimated the length scale by n^i so there are $n^{i(d-1)}$ decorations at this stage, and each gives a free energy contribution $\delta\mathcal{F}(L/n^i)$. Hence, the total free energy of all the decorations will be

$$\delta\mathcal{F}^{\mathrm{Tot}}(L) = \sum_{i=0}^{k} n^{i(d-1)} \delta\mathcal{F}\left(\frac{L}{n^i}\right) \tag{37}$$

with k as above.

In this way, then, we can estimate the effect of wall roughening on all length scales up to L, and remove the restriction that the wall shape must be smooth. Such generalizations are crucial to get the correct marginality breaking free energy, as we shall see.

3.1.4. Scaling and criticality in $d = 2$ and $= 2 + \epsilon$. The preceding results can now be used to construct the RG transformation in $d = 2 + \epsilon$. This allows us to investigate the marginality breaking effect of domain wall roughening in two dimensions, and to investigate the behaviour of the $h = 0$ fixed point as we move away from $d = 2$.

Using (37) and the free energy forms found in the previous sections, a full decoration of the domain walls may be done in general dimension $d \geqslant 2$. For the sake of generality we will use the general form of the wall free energy given by (24*a*):

$$\delta\mathcal{F}^{\mathrm{Tot}} = -\tilde{c}\left(\frac{c_0 h}{J}\right)^{\gamma} L^{\theta} \sum_{i=0}^{k} n^{i(d-1-\theta)}. \tag{38}$$

From the values of θ given in table 3, the summand is

$$n^{i(d-1-\theta)} = \begin{cases} n^{i((2d-4)/3)} = 1 + i\frac{2}{3}\epsilon \ln n & \text{continuum} \\ n^{i(2d-4)} = 1 + i2\epsilon \ln n & \text{lattice} \end{cases}$$

for $d = 2 + \epsilon$. To further simplify matters we define the coefficient

$$\phi = \begin{cases} \frac{2}{3} & \text{continuum} \\ 2 & \text{lattice.} \end{cases} \tag{39}$$

Then, the total free energy of the wall decorations may be concisely written as

$$\frac{\delta\mathcal{F}^{\mathrm{Tot}}}{J} = -\tilde{c}\left(\frac{c_0 h}{J}\right)^{\gamma} L^{\theta}\left[(k+1) + \epsilon\phi(\ln n)\frac{k(k+1)}{2}\right]. \tag{40}$$

This result may be compared both with that of Villain [7] and Grinstein and Ma [8] who find $\delta\mathcal{F}^{\mathrm{Tot}} \sim h^{4/3} L \ln L$ for $d = 2$ using a continuum interface model, and with the result of Binder [30] who finds $\delta\mathcal{F}^{\mathrm{Tot}} \sim h^2 L \ln L$ in a $2d$ lattice calculation. Both these results agree with (40) with the appropriate choice of the exponents γ and θ (see table 3).

The wall decorations reduce the effective surface tension of the domains. As a result, the average domain size will decrease. We can quantify this result by rewriting the free energy of the entire strip as

$$\mathcal{F} = \left(\frac{N}{\Xi_L}\right)(2JL^{d-1} - c_0 h\sqrt{\Xi_L L^{d-1}} + \delta\mathcal{F}^{\mathrm{Tot}}). \tag{41}$$

Here, we used the flat wall result (3) as a model, but noted the fact that there is, on average, a further contribution of $\delta\mathcal{F}^{\mathrm{Tot}}$ per domain wall from the decorations.

Extremalizing this free energy with respect to Ξ_L gives the average domain size as

$$\Xi_L = \left(\frac{c_0 h}{J}\right)^{-2} L^{d-1}\left(1 + \frac{\delta \mathcal{F}^{\mathrm{Tot}}}{J L^{d-1}}\right). \tag{42}$$

As expected, the domain size is reduced by interface roughening.

This correction to the correlation length Ξ_L also has implications for the phenomenological RG equation. This equation obtained from (2) with the use of (42) and (6) is now quite complex, but it can be simplified by linearizing in ϵ and using small h/J. After some tedious algebra, one finds the following RG equation:

$$h' = h\left(1 + ch^{\gamma}\frac{\ln b}{\ln n} - \frac{\epsilon}{2}\ln b\right) \tag{43}$$

where $c \equiv \tilde{c}c_0^{\gamma}$ and we have let $J = 1$ for simplicity. This has an unstable fixed point at

$$h^* = \left(\frac{\epsilon \ln n}{2c}\right)^{1/\gamma} + O(\epsilon^2)^{1/\gamma} \tag{44}$$

which remains in the small h region of validity of our description since ϵ is regarded as small. The eigenvalue of (43) is given by

$$\left.\frac{\partial h'}{\partial h}\right|_{h=h^*} = 1 + \frac{1}{2}\gamma\epsilon \ln b + \mathcal{O}(\epsilon^2) = b^{1/\nu}.$$

This yields the critical exponent

$$\nu = \frac{2}{\epsilon\gamma} \tag{45}$$

which characterizes the scaling of the bulk correlation length, $\xi \sim |h - h^*|^{-\nu}$. The arbitrary scale variable n disappears from the critical exponent ν, which is a universal quantity, though it remains through a weak logarithmic dependence in h^* and other non-universal quantities.

For $d = 2$ we must go back to equation (43) with $\epsilon = 0$:

$$h' = h\left(1 + ch^{\gamma}\frac{\ln b}{\ln n}\right). \tag{46}$$

This is equivalent (at small h) to

$$\exp\left(\frac{\ln n}{\gamma c (h')^{\gamma}}\right) = \frac{1}{b}\exp\left(\frac{\ln n}{\gamma c h^{\gamma}}\right). \tag{47}$$

This is the same form as the standard rescaling of a correlation length $\xi(h') = b^{-1}\xi(h)$, so the correlation length is

$$\xi \sim \exp\left(\frac{A}{h^{\gamma}}\right) \tag{48}$$

close to the fixed point $h^* = 0$, where A is the non-universal constant $\ln n/(c\gamma)$.

The results of these calculations are summarized in table 4.

Here the exponent is $\gamma = 4/3$ for the continuum or $\gamma = 2$ for the lattice. Our results for the continuum are identical to those given in [32]. This is because the fixed-point structure of (43) is very similar to that found there from the scaling of the surface tension (while ours comes from the phenomenological rescaling of correlation lengths). The lattice results agree with those of [29, 30, 54].

Putting $\epsilon = 1$ in (45) one gets, for the lattice, $\nu = 1$ in unexpectedly good agreement with recent Monte Carlo results in $d = 3$ [55], $\nu = 1.02 \pm 0.06$. Of course such an extrapolation must not be given much weight, as ϵ is assumed to be $\ll 1$ in the theory.

Table 4. Main results of the flat wall analysis.

Dimensions	Fixed point	Bulk correlation length
2	$h^* = 0$	$\xi \sim \exp(A/h^\gamma)$
$2+\epsilon$	$h^* = \left(\frac{\epsilon \ln n}{2c}\right)^{1/\gamma}$	$\xi \sim (h-h^*)^{-2/\epsilon\gamma}$

3.2. Low-temperature theory

The effect of the zero-temperature wall roughening on the surface tension is (by (41)) equivalent to the replacement of J by

$$\tilde{J} = J + \frac{\delta \mathcal{F}^{\mathrm{Tot}}}{2L^{d-1}}. \tag{49}$$

Consequently, the low-temperature analyses given in sections 2.2 and 2.3.2 have to be modified by the replacement $J \to \tilde{J}$, in equations (10)–(14) and (20) and (21).

The roughening also affects the entropy since it increases the number of possible configurations. The entropy change can be obtained crudely by a slight generalization of the counting used to derive (37), or by a more complete analysis given elsewhere [56].

As remarked in section 2.2, the zeroth-order thermal scaling (13) is not marginal in $d > 1$, and so the modifications just discussed do not change the RG thermal flow directions for h small and d near 2. So the ϵ-expansion results of section 3.1.4 can be combined with those of section 2.2 to infer the flow diagrams shown in figure 11 for $d = 1, 2, 2+\epsilon$. For $d = 2+\epsilon$ this implies a second-order phase transition at the phase boundary shown, inside which (i.e. at small h, T) long-range order occurs for $h \neq 0$. This is consistent with previous renormalization group discussions [12, 34].

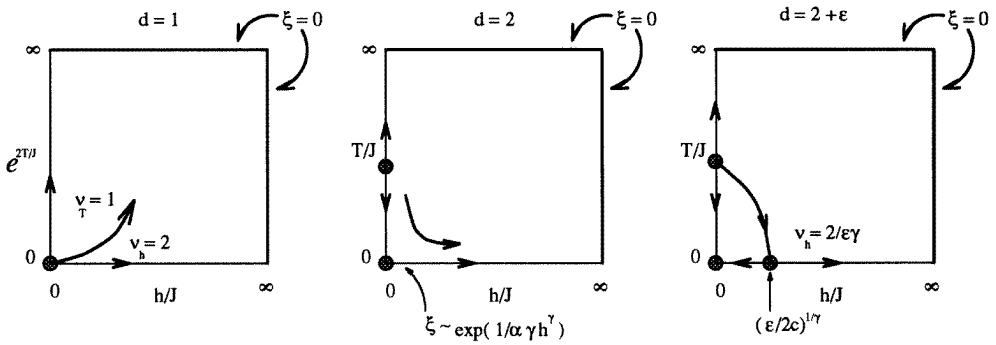

Figure 11. The RG flow diagram for the RFIM as predicted by our finite-size scaling analysis.

The extended theory outlined in the first two paragraphs above provides the low-temperature free energy modifications produced by rough walls.

This suggests the possibility of distinguishing wall roughening effects by comparing numerical data on free energy with this theory extended as just outlined. This comparison has been made with the transfer matrix free energy data discussed in section 2.3.2. Despite the excellent quality of the data, and their remarkably good agreement with the flat wall theory, it was not found possible to extract wall roughening effects from them. This is because the statistical fluctuations in the data, although extremely small, are nevertheless

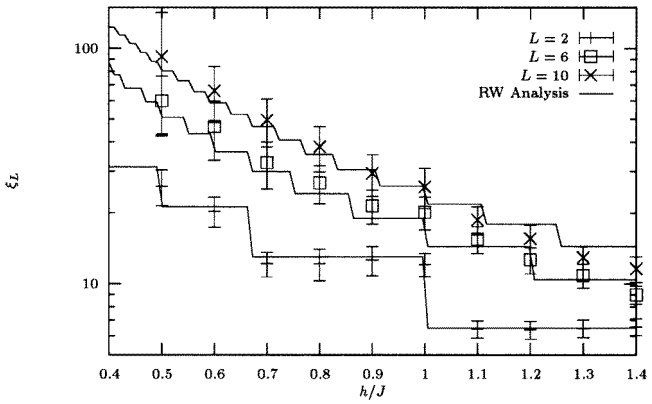

Figure 12. The domain size as a function of h/J at $T = 0$ determined by the max-flow algorithm (data points), and the flat wall analysis (lines) for a binary field distribution.

greater than the roughening contributions in the ranges of parameters appropriate for the validity of the theory (ensuring $\xi \gg L$). So, we turn to other more sensitive comparisons.

3.3. Numerics: correlation and roughening characteristics from the max-flow ground-state algorithm

This section describes the extraction of domain wall roughening characteristics from data obtained using the max-flow algorithm for constructing ground states.

One comparison uses domain-size correlation length data, which are much more sensitive than the free energy to domain wall roughening, particularly in wide strips because of the crucial role of roughening in the marginal dimension of $d = 2$. The other involves direct measures of the wall wandering. These measures are the average over many walls, (for a given h and base scale L) of the maximum height (wandering excursion) $b_{\max}$, or of the root-mean-square height $b_{\rm rms}$.

Both binary and Gaussian random field distributions were used. As expected, the Gaussian distribution gives smoother dependences, and has provided the most useful data. However, the binary results have some interesting features, as we now briefly show. Figure 12 gives numerical data for the configurationally averaged domain size. A 'stepping' of the data as a function of h is apparent, particularly for smaller L. This is predicted by the flat wall description (appendix A) equations (A6), (A8) since in (A8), $q = (2 + \lfloor (2JL)/h \rfloor)^{-1}$ involves the integer part function $\lfloor\ \rfloor$. There is also a certain discreteness implied in the use of the transfer matrix. For comparison, the flat wall theory is shown in the figure. The flat-wall random-walk analysis also compares very satisfactorily with corresponding domain size data (figure 9) from the Gaussian distribution. Here, the data contain no steps. If one repeats the random walk analysis with a Gaussian distribution, the 'integer part' function does not occur, and the transfer matrix becomes a convolution operator. Since the eigenfunctions are again plane waves, the final result for the correlation length is the same, except that it has no 'integer part' function, and thus no 'stepping'. However, though the Gaussian distribution must therefore set the large length scale behaviour, in energy (figure 3) and domain size (above) there can be real differences for these quantities between binary and Gaussian cases at smaller scales.

The domain size data can be fitted to the flat wall theory or to the analysis including

wall roughening (sections 3.1.3, 3.1.4). Equation (4) gives the basic flat wall description, in which for strips ($d = 2$), $\Xi_L \sim Lh^{-2}$, and one fitting coefficient (c_0) occurs. The fuller random walk version of the flat wall theory (section 2.1.4) is equivalent, for small h/L, but more generally it gives a Ξ_L different by a 'discreteness factor' $(1 + \mathcal{O}(h/L))$. The wall roughening analysis instead corrects the flat wall Ξ_L by a factor $(1 + \mathcal{O}(h^\gamma L^{\theta-d+1} \ln L))$. This should be amalgamated with the discreteness factor evident from the RW analysis. Then the domain wall roughening theory gives the best quality of fit to the max-flow data on Ξ_L. For instance, considering a Gaussian random field distribution, table 5 shows the decreased statistical error χ^2 associated with the addition of this domain roughening term. Even though this extra term provides an extra free constant to the fit ($c = \tilde{c}c_0^\gamma$), it does not necessarily decrease χ^2. Indeed, it worsens the fit to the zeroth-order theory since the higher-order 'discreteness term' has been neglected. When this term is ignored, the roughening only has a correlation coefficient of $r = 0.218$. However, when this discreteness term has been included from the more complete random walk analysis, the wall roughening is seen to decrease the value of χ^2. It then has a much more significant correlation coefficient of $r = 0.816$.

Table 5. Results of fits to the $T = 0$ domain size data.

	Flat domain walls		Roughened domain walls	
	Zeroth-order	Random walk	Zeroth-order	Random walk
χ^2	4.215	0.607	4.447	0.404

The max-flow data in the wall decoration variables $b_{\rm rms}$, $b_{\rm max}$ give much more conclusive evidence for the roughening effects and provide quantitative estimates of exponents. Data for the h-dependence of $b_{\rm rms}$ for $L = 8$ are shown in figure 16 for both binary and Gaussian distributions. Again, the jagged character of the binary result is evident, even at this moderately large L. So the remaining discussion is confined to the Gaussian case. To compare with the prediction (24*b*), a log–log plot of the Gaussian $b_{\rm rms}$ versus h is given for $L = 2, \ldots, 11$ in figure 15. A very similar plot is obtained also for $b_{\rm max}$, though the absolute size of $b_{\rm max}$ is larger, by up to a factor of 4. The departure from linearity of the log–log plot at small h is almost certainly a lattice effect. That requires $b \gtrsim 1$, and using e.g. (26) (with $c_0 = 1.8$) to estimate where $b \approx 1$ suggests that (24*b*) should break down for $h/J \lesssim 5L^{-1/2}$, which is in qualitative agreement with what is seen. Similarly, a breakdown of the simple theory giving (24*b*) is expected when b (strictly $b_{\rm max}$) becomes comparable to Ξ_L, i.e. (using (26) and (4)) for $h/J \gtrsim 1.5$. This L-independent cutoff is consistent with the departures from linearity seen at the largest fields in the log–log plot. The scaling window between the upper and lower h departures is quite wide for the largest Ls, and consequently they should give the most accurate field exponent κ from power law fits to (24*b*) within the scaling window. The results, from both $b_{\rm rms}$ and $b_{\rm max}$ are shown in figure 13 and are consistent with $\kappa \approx 2.1 \pm 0.3$. Figure 14 shows the L-dependent prefactor of h^κ in $b_{\rm rms}$ and $b_{\rm max}$. In each case, the prefactor is very close to linear in L in the larger L scaling regime, consistent with $\zeta = 1$ in (24*b*). The behaviours seen in figure 15, and in the corresponding plot for $b_{\rm max}$, as well as the associated exponents κ, ζ are therefore consistent with the analysis in section 3.1.

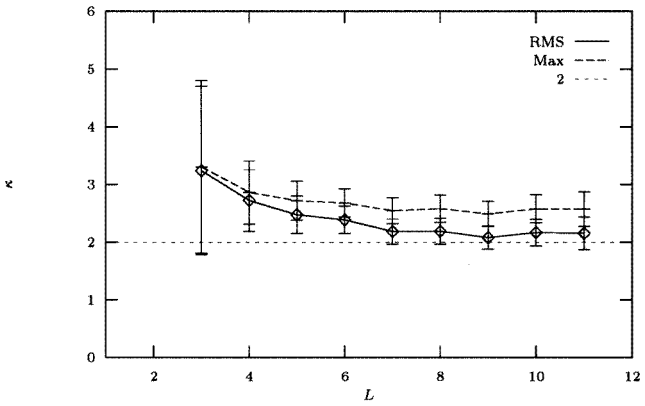

Figure 13. The wall roughening exponent κ as determined from power law fits to $b_{\rm rms}$ and $b_{\rm max}$. For large L, these tend towards 2.

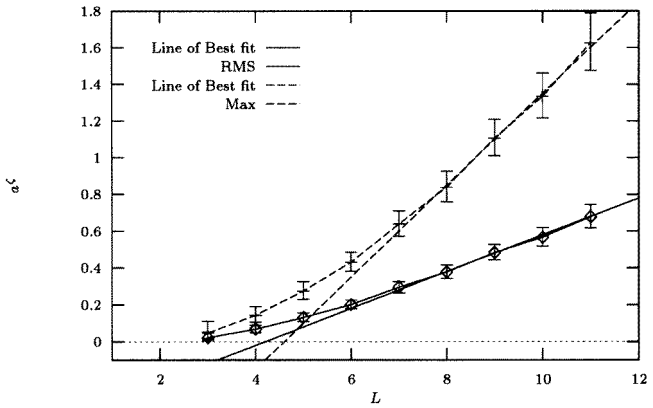

Figure 14. The wall roughening term a^ζ as determined from power law fits to $b_{\rm rms}$ and $b_{\rm max}$. For large L, these tend towards a linear dependence on L, consistent with $\zeta = 1$, as shown by the lines of best fit.

4. Conclusions

In this paper we have developed a domain scaling description for the random field Ising model by exploiting a bar geometry. As in earlier work of Villain [7], Grinstein and Ma [8] and Binder [30], the marginality of the basic flat-wall picture at the lower critical dimension $d_{\rm l} = 2$ is removed by wall roughening effects (section 3). The resulting phenomenological renormalization group transformation has been used to obtain the critical properties. In particular, the special critical behaviour of the two-dimensional correlation length and the phase diagram in $d = 2 + \epsilon$ have been given (section 3.1.4).

The wall roughening ingredient has its own scaling characteristics (the exponents γ, θ, κ, ζ) which have been here rederived using both a simple analytical method (following Nattermann [47, 48]) and a field theoretic approach. These exponents have a direct bearing upon the RG transformation and hence on the scaling properties.

An essential element to this study has been the support that numerical studies have provided for the analytic description. The comparison between numerical data and analytic

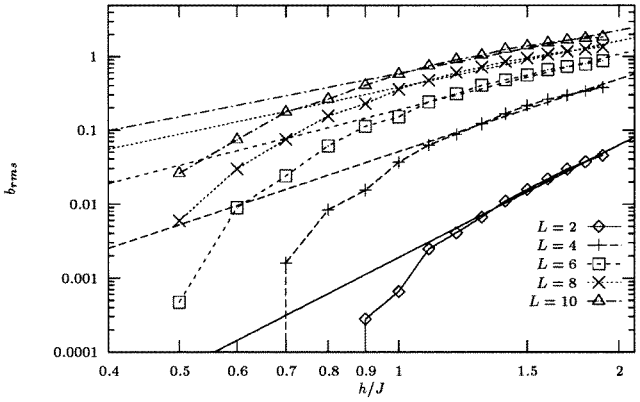

Figure 15. The root-mean-square domain wall width as a function of h/J for various length scales L. The use of a log–log plot shows the scaling window where the plots are linear.

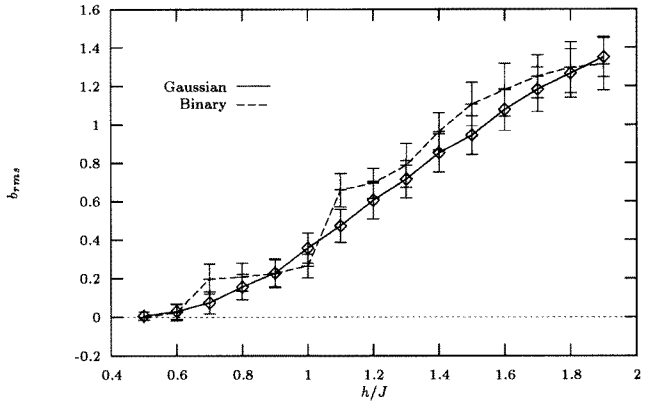

Figure 16. The rms domain wall width as a function of h/J for $L = 8$. This plot emphasizes the difference between the binary and Gaussian random field distributions, showing the stepped nature of the former as more excitations become favourable at lower h/J.

predictions was made in the strip geometry so that the critical ingredients of the theory could be directly investigated. These ingredients include the domain size, the free energy, and the roughening characteristics, as functions of h, T and strip width L.

The numerical approaches employed were transfer matrix and Monte Carlo techniques, and a ground-state (max-flow) algorithm. The first two give free energy and domain size data confirming the basic flat-wall picture through: (i) the h^2/L dependence of the $T = 0$ flat-wall energy at low h, and its low-temperature generalization; (ii) the domain size distribution and the correlation length–domain size relationship.

The numerical ground-state data, obtained via the max-flow algorithm, not only directly verify the basic validity of the domain size predicted by the (flat wall) random walk analysis, but they also provide evidence for the roughening effects in the domain size. The max-flow data on the wall decoration variables $b_{\rm rms}$, $b_{\rm max}$ are the most conclusive evidence for roughening effects. They give power law scaling in a window of the size predicted by the theory, sufficient at large L to give quite accurate values for roughening exponents, in good agreement with the (lattice based) theory.

The conclusions is that the theory contains the correct ingredients, and the numerical data provide quantitative confirmations of the way they enter into the theory.

We have not made corresponding numerical investigations of the $d = 3$ case, where it is of course more difficult to obtain data for the range of L's we needed here. However, we hope the present work may stimulate such an effort, which (e.g. using the ground-state algorithm) could sort out the so far unresolved critical behaviour [13, 14]. Another extension, presently under consideration, is to the kinetic behaviour, for which the free energy scaling discussed here is an essential ingredient.

Acknowledgments

We would like to thank T Nattermann for interesting comments. SLAdQ thanks the Department of Theoretical Physics at Oxford, where this work was initiated, for the hospitality, and the cooperation agreement between Academia Brasileira de Ciências and the Royal Society for funding his visit. Research of SLAdQ is partially supported by the Brazilian agencies Ministério de Ciência e Tecnologia, Conselho Nacional de Desenvolvimento Científico e Tecnológico and Coordenação de Aperfeiçoamento de Pessoal de Ensino Superior.

Appendix A. Exact correlation length on strips at $T = 0$

We consider the connected correlation function

$$\chi_{il} = \langle \sigma_i \sigma_{i+l} \rangle - \langle \sigma_i \rangle \langle \sigma_{i+l} \rangle. \tag{A1}$$

At $T = 0$ the thermodynamic average becomes an average over the possible ground states of the system.

In considering the ground state of the RFIM, one notes that even if the field is small, the energy to create a domain wall, $2JL$, can be accumulated from fluctuations in the random field over large domains. In $d \leqslant 2$ the L dependences are such that this result persists in the $L \to \infty$ limit [1].

With this in mind, let us define the quantity

$$\mathcal{S}(k, l) = \sum_{j=k}^{k+l} \sum_{i=1}^{L} h_{ij} \tag{A2}$$

where i labels the vertical coordinate on the strip, and j the horizontal one. Whenever $|\mathcal{S}(k, l)| \geqslant 4JL$, it is favourable to insert a domain wall at positions k and $k + l$. When we attempt to employ this algorithm on a variety of field configurations, one immediately notices that the ground state is still not completely determined.

A region between two opposite random fields, and with endpoints k, j such that $S(k, j) = 0$ (and j is the site closest to k when this is so) is a 'floppy domain' (FD) in the sense that in an average over the ground states, the spins in these domains may point up or down, and are not fixed like the spins in other regions ('rigid domains' (RD)).

There is increased degeneracy if $2JL/h$ is an integer, because the conditions for both $\uparrow\downarrow$ and $\downarrow\uparrow$ FD can be simultaneously satisfied. To avoid the additional difficulties of this case, we shall assume that $2JL/h$ is not an integer.

The degeneracy in the ground state gives rise to non-vanishing connected correlations. Indeed, it is the FDs that contribute exclusively to χ_{il}. If either σ_i or σ_{i+l} is in an RD then $\langle \sigma_i \sigma_{i+l} \rangle = \langle \sigma_i \rangle \langle \sigma_{i+l} \rangle$. Furthermore, if the two spins are in different FD, they are

uncorrelated random variables, and their contribution to χ_{il} also vanishes. Thus, one need only consider spins that are in the same FD.

We have three effects to consider.

(i) The probability $\mathcal{W}_1(\tilde{l})$ that there exists an FD of size $\tilde{l} > l$.

(ii) Given that σ_i is in an FD, the probability $\mathcal{W}_2$ that the σ_{i+l} is also in the FD.

(iii) The thermal average and the average over random field configurations subject to the constraint that the spins σ_i and σ_{i+l} are both in the same FD. We label this probability $\mathcal{W}_3$.

We also introduce the variable

$$\mathcal{L} = \left\lfloor \frac{2JL}{h} \right\rfloor + 1$$

where $\lfloor x \rfloor$ denotes the integer part of the non-integer x.

We can view the random field configuration on a strip of width L as a random walk in $1+1$ dimensions. At each site along the horizontal direction of the strip, the walk changes by a height equal to the columnar sum of random field values at that point. Using this view, $\mathcal{S}(0, l)$ represents the height of the random walk at $x = l$.

If the aggregated change in height of the random walk ever reaches $\mathcal{L}$ then we have accumulated enough parallel fields to form a domain. If there are regions between these peaks where the change in height is zero, then these are FD.

In this random walk picture, $\mathcal{W}_1(\tilde{l})$ is the probability that the random walk returns to the origin after taking $\tilde{l}$ steps, which is known to fall off exponentially with l,

$$\mathcal{W}_1(l) \sim \exp\left[\frac{-l}{\xi_L(\mathcal{L})}\right] \tag{A3}$$

where $\xi_L(\mathcal{L})$ is a characteristic decay length to whose exact determination we shall return in a moment.

From geometrical considerations, $\mathcal{W}_2 \sim 1/l$. For the third probability, we note that the average over ground states corresponds to an average over domain wall positions. Since the number of places for a domain wall to be inserted between two spins separated by a distance l goes like l, we could estimate the conditional probability $\mathcal{W}_3$ as $\sim 1/l^2$. These are only rough estimates, the probabilities depend also upon the ratio h/J. But we only need here the l dependence, and the important feature of $\mathcal{W}_2$ and $\mathcal{W}_3$ is their power law decay in l. We conclude that the only exponential contribution is from $\mathcal{W}_1(l)$, and this gives the exponential decay of χ, so the $\xi_L(\mathcal{L})$ defined by (A3) is actually the correlation length.

Now $\mathcal{W}_1(\tilde{l})$ is the probability that a directed random walker in $1+1$ dimensions returns to the origin after $\tilde{l}$ steps, without hitting walls at $\pm\mathcal{L}$. We solve this problem by reference to the transfer matrix formalism of random walks [57]. This involves writing down a transfer matrix $T(n, m)$ with $n, m \in \{1, 2, \ldots, \mathcal{L}\}$ which represents the probability that the random walker makes a step from position m to n. In terms of the RFIM, this means that

$$T(n, m) = \text{Prob}\left(\sum_{i=1}^{L} h_{ij} = (n-m)h\right). \tag{A4}$$

The leading eigenvalue of the transfer matrix, $\lambda(\mathcal{L})$ is related to the survival probability by

$$\mathcal{W}_1(l) \sim \lambda(\mathcal{L})^l \tag{A5}$$

so that the correlation length of equation (A3) is

$$\xi_L(\mathcal{L}) = \frac{-1}{\ln \lambda(\mathcal{L})}. \tag{A6}$$

For $L = 1$, the transfer matrix is (using (A4)) tridiagonal and symmetric, with zeros on the diagonal and 1/2 on the neighbouring off diagonals. We can generalize this result for all L, by noting a general pattern in a *row* through the middle of the transfer matrix:

$(i-j)$	...	4	3	2	1	0	+1	+2	+3	+4	...
$L=1$	...	0	0	0	$\frac{1}{2}$	0	$\frac{1}{2}$	0	0	0	...
$L=2$	...	0	0	$\frac{1}{4}$	0	$\frac{2}{4}$	0	$\frac{1}{4}$	0	0	...
$L=3$	...	0	$\frac{1}{8}$	0	$\frac{3}{8}$	0	$\frac{3}{8}$	0	$\frac{1}{8}$	0	...
$L=4$	...	$\frac{1}{16}$	0	$\frac{4}{16}$	0	$\frac{6}{16}$	0	$\frac{4}{16}$	0	$\frac{1}{16}$	...
$\vdots$											

The numerators of the elements follow the same pattern as the numbers in Pascal's triangle, and the denominators are simply 2^L. This is due to the Gaussian nature of the random walk whereby $T_L(n,m) = [T_1(n,m)]^L$. These matrices are all diagonalized by the same type of vectors:

$$\mathbf{\Phi}_j = \sin(j\pi q) \tag{A7}$$

where the wavenumber q is chosen to be consistent with the boundary conditions of the matrix, i.e. $q = n/(\mathcal{L}+1)$. The pattern of entries in the transfer matrix gives the eigenvalues of these vectors as

$$\lambda = \cos^L(q\pi). \tag{A8}$$

Clearly, the largest eigenvalue is the one with $q = q_1 = 1/(\mathcal{L}+1)$. If h is small, then $\mathcal{L}$ is large and q_1 is small so that equation (A6) gives the correlation length as

$$\begin{aligned}\xi_L &= \frac{1}{L\ln\cos(\pi/(2J/h+2))} \\ &= 2L\left(\frac{2J}{\pi h}\right)^2 + \frac{16\pi^2}{h} + \mathcal{O}(1).\end{aligned} \tag{A9}$$

Appendix B. Full field theory of domain interfaces

We use a $(d-1)$-dimensional Cartesian coordinate system placed on the hyperplane where the flat interface would have been. Then, the deviation of the domain wall from this hyperplane is given by the function $P(\boldsymbol{x})$. Using the model of equation (1), this decoration has a free energy at $T = 0$ of

$$\mathcal{F}[P(\boldsymbol{x}), \nabla P(\boldsymbol{x})] = 2J\int\sqrt{1+(\nabla P)^2}\,\mathrm{d}^{d-1}\boldsymbol{x} - c_0 h\sqrt{\int P(\boldsymbol{x})\,\mathrm{d}^{d-1}\boldsymbol{x}} \tag{B10}$$

where both integrals are over the hyperplane defined by $x_i \in [0, L]$. This free energy is minimized via the generalized Euler–Lagrange equation:

$$\sum_{i=1}^{d-1}\frac{\partial}{\partial x_i}\frac{\delta\mathcal{F}}{\delta(\partial P(\boldsymbol{x})/\partial x_i)} = \frac{\delta\mathcal{F}}{\delta P(\boldsymbol{x})}. \tag{B11}$$

Note that the right-hand side is a constant, and define it as

$$N_0 J = \frac{-c_0 h}{4\sqrt{\int P(\boldsymbol{x})\,\mathrm{d}^{d-1}\boldsymbol{x}}}. \tag{B12}$$

This leads to a rather complicated d-dimensional differential equation.

$$N_0 = \sum_{i=1}^{d-1} \frac{\left\{ \partial_i^2 P[1 + (\nabla P)^2] - \sum_{j=1}^{d-1} \partial_i P \partial_j P \partial_{ij} P \right\}}{[1 + (\nabla P)^2]^{3/2}}. \tag{B13}$$

Here, $\partial_i \equiv \frac{\partial}{\partial x_i}$.

To simplify things we consider the isotropic solution, which only depends on the radial coordinate $r^2 = \sum_{i=1}^{d-1} x_i^2$.

Then, with $\partial_r P(\boldsymbol{x}) \equiv P'(r)$ the isotropic equation becomes

$$N_0 = \frac{((d-2)/r)P'(r)(1 + P'(r)^2) + P''(r)}{(1 + P'(r)^2)^{3/2}}. \tag{B14}$$

Note that this equation may alternatively be obtained by extremalizing an isotropic free energy functional,

$$\delta\mathcal{F}[P(r), P'(r)] = 2J\Omega \int \sqrt{1 + P'(r)^2} r^{d-2}\, \mathrm{d}r - c_0 h \sqrt{\Omega \int P(r) r^{d-2}\, \mathrm{d}r}. \tag{B15}$$

Here

$$\Omega = \frac{\pi^{(d-1)/2}}{((d-1)/2)!}(d-1) \tag{B16}$$

is the area of the $(d-1)$-dimensional unit ball. However, in the more general case the isotropic solution is a member of the larger set of optimal solutions.

It may be checked by direct substitution that the solution to the wall decoration problem encapsulated in equations (B12) and (B14) is a hypersphere of radius R

$$P(r) = \sqrt{R^2 - r^2} - P_0 \tag{B17}$$

where R satisfies the requirement $-1/R = N_0$. The constant P_0 is determined by the choice of the boundary conditions $P(r = L/2) = 0$

$$P_0 = \sqrt{R^2 - \left(\frac{L}{2}\right)^2}. \tag{B18}$$

In addition, the constraint (B12) imposes the self-consistency relation

$$R^2 = \frac{J^2(d-1)^2 4(\delta V)}{c_0^2 h^2} \tag{B19}$$

which we use to determine $R(h)$. Here δV is the extra volume added by the decoration $\delta V = \Omega \int_0^{L/2} P(r) r^{d-2}\, \mathrm{d}r$.

Thus, (B19) is difficult to solve for $R(h)$. However, we are interested in the regime $h/J < 1$ where we expect the decorations to be small ($R \gg L$) and we may expand in powers of L/R. To first order in $1/R$ the excess volume and area are

$$\delta V = \frac{\Omega}{R(d^2-1)} \left(\frac{L}{2}\right)^{d+1} \tag{B20}$$

$$\delta A = \frac{\Omega}{2R^2(d+1)} \left(\frac{L}{2}\right)^{d+1}. \tag{B21}$$

Then, equation (B19) gives the equilibrium radius as

$$R = \left(\frac{c_0 h}{J}\right)^{-2/3} L^{(d+1)/3} \left(\frac{4\Omega(d-1)}{2^{d+1}(d+1)}\right)^{1/3}. \tag{B22}$$

Inserting the first-order forms (B20) and (B21) evaluated at the equilibrium radius (B22) into (B10) then gives the first order free energy fluctuation

$$\mathcal{F}_{\rm wall}(L) = -\tilde{c}\left(\frac{c_0 h}{J}\right)^{4/3} L^{(d+1)/3} + \mathcal{O}(h^{8/3}). \tag{B23}$$

Here $\tilde{c}$ is the numerical constant

$$\tilde{c} = \left[\frac{\Omega^{1/3}}{(d+1)^{1/3}(d-1)^{2/3}}\right]\left[\frac{-2^{-1/3}+2^{8/3}}{2^{(d+7)/3}}\right] \tag{B24}$$

and is positive for all $d > 1$. This shows that wall roughening is always favourable for $d \geqslant 2$.

Finally, the wall wandering height is

$$b \equiv P(r=0) \sim h^{2/3} L^{(5-d)/3} + \mathcal{O}(h^{8/3}). \tag{B25}$$

References

[1] Imry Y and Ma S-K 1975 *Phys. Rev. Lett.* **35** 1399
[2] Grinstein G 1976 *Phys. Rev. Lett.* **37** 944
[3] Aharony A, Imry Y and Ma S-K 1976 *Phys. Rev. Lett.* **37** 1364
[4] Young A P 1977 *J. Phys. A: Math. Gen.* **10** L257
[5] Aharony A 1978 *Phys. Rev.* B **18** 3318
[6] Aharony A 1978 *Phys. Rev.* B **18** 3328
[7] Villain J 1982 *J. Physique Lett.* **43** L551
[8] Grinstein G and Ma S-K 1982 *Phys. Rev. Lett.* **49** 685
[9] Imbrie J 1984 *Phys. Rev. Lett.* **53** 1747
[10] Bricmont J and Kupiainen A 1987 *Phys. Rev. Lett.* **59** 1829
[11] Aizenman M and Wehr J 1989 *Phys. Rev. Lett.* **62** 2503
[12] Nattermann T and Villain J 1988 *Phase Transitions* **11** 5
[13] Rieger H 1995 *Phys. Rev.* B **52** 6659
[14] Gofman M, Adler J, Aharony A, Harris A B and Schwartz M 1996 *Phys. Rev.* B **53** 6362
[15] Fishman S and Aharony A 1979 *J. Phys. C: Solid State Phys.* **12** L729
[16] Yoshizawa H, Cowley R A, Shirane G, Birgeneau R J, Guggenheim H J and Ikeda 1982 *Phys. Rev. Lett.* **48** 438
[17] Belanger D, King A, Jaccarino V and Cardy J L 1983 *Phys. Rev.* B **28** 2522
[18] Shapira Y, Oliveira N F Jr and Foner S 1984 *Phys. Rev.* B **30** 6639
[19] Birgeneau R J, Cowley R A, Shirane G and Yoshizawa H 1985 *Phys. Rev. Lett.* **54** 2147
[20] Yoshizawa H, Cowley R A, Shirane G and Birgeneau R J 1985 *Phys. Rev.* B **31** 4538
[21] Mitchel P, Cowley R A, Yoshizawa H, Böni P, Uemura Y J and Birgeneau R J 1986 *Phys. Rev.* B **34** 4719
[22] Geschwind S, Ogielski A T, Devlin G and Hegarty J 1988 *J. Appl. Phys.* **63** 3291
[23] Ramos C A, King A and Jaccarino V 1988 *Phys. Rev.* B **37** 5483
[24] Ferreira I, King A and Jaccarino V 1991 *Phys. Rev.* B **43** 10797
[25] Lederman M, Selinger J V, Bruinsma R, Hamman J and Orbach R 1992 *Phys. Rev. Lett.* **68** 2086
[26] Becerra C C and Paduan-Filho A 1993 *J. Appl. Phys.* **73** 5491
[27] Hill J, Feng Q, Birgeneau R J and Thurston T 1993 *Phys. Rev. Lett.* **70** 3655
[28] Hill J, Thurston T R, Ramstad M, Erwin R W and Birgeneau R J 1991 *Phys. Rev. Lett.* **66** 3281
[29] Grinstein G and Ma S-K 1983 *Phys. Rev.* B **28** 2588
[30] Binder K 1983 *Z. Phys.* B **50** 343
[31] Villain J 1985 *J. Physique* **46** 1843
[32] Nattermann T 1985 *Phys. Status Solidi* b **131** 563
[33] Stinchcombe R B, Moore E D and de Queiroz S L A 1996 *Europhys. Lett.* **35** 295
[34] Bray A J and Moore M 1985 *J. Phys. C: Solid State Phys.* **18** L927
[35] Moore E D 1995 *DPhil Thesis* Department of Theoretical Physics, University of Oxford (unpublished)
[36] Ogielski A 1986 *Phys. Rev. Lett.* **57** 1251
[37] da Cruz H and Stinchcombe R B 1986 *J. Phys. C: Solid State Phys.* **19** 3555
[38] Farhi E and Gutmann S 1993 *Phys. Rev.* B **48** 9508

[39] Schwarz M and Sherrington D 1985 *J. Phys. C: Solid State Phys.* **18** L817
[40] Schwartz M and Soffer A 1985 *Phys. Rev. Lett.* **55** 2499
[41] de Queiroz S L A 1995 *Phys. Rev.* E **51** 1030
[42] Crisanti A, Nicholis S, Paladin G and Vulpiani A 1990 *J. Phys. A: Math. Gen.* **23** 3083
[43] Derrida B 1984 *Phys. Rep.* **103** 29
[44] Goldberg A 1985 Internal report MIT/LCS/TM-291, Laboratory for Computer Science, Massachusetts Institute of Technology (unpublished)
[45] Picard J and Radcliffe H 1974 *Networks* **5** 357
[46] Press W, Flannery B, Teukolsky S and Vetterling W 1994 *Numerical Recipes in C, The Art of Scientific Computing* 2nd edn (Cambridge: Cambridge University Press)
[47] Nattermann T 1984 *Z. Phys.* B **54** 247
[48] Nattermann T 1985 *Phys. Status Solidi* b **132** 125
[49] Grinstein G 1984 *J. Appl. Phys.* **55** 2371
[50] Parisi G and Sourlas N 1979 *Phys. Rev. Lett.* **43** 744
[51] Mézard M and Parisi G 1990 *J. Phys. A: Math. Gen.* **23** L1229
[52] Mézard M and Young A P 1992 *Europhys. Lett.* **18** 653
[53] Fernandez J, Grinstein G, Imry Y and Kirkpatrick S 1983 *Phys. Rev. Lett.* **51** 203
[54] Aharony A and Pytte E 1983 *Phys. Rev.* B **27** 5872
[55] Newman M E J and Barkema G T 1996 *Phys. Rev.* E **53** 393
[56] Moore E 1995 preprint cond-mat 9505061, accepted for publication in *Phys. Rev.* E
[57] Privman V and Švrakić N 1989 *Directed Models of Polymers, Interfaces and Finite-Size Properties (Lecture Notes in Physics 338)* (Berlin: Springer)